

Self-Assembled Multivalent DNA Nanostructures for Noninvasive Intracellular Delivery of Immunostimulatory CpG Oligonucleotides

Jiang Li,[†] Hao Pei,[†] Bing Zhu,[†] Le Liang, Min Wei, Yao He, Nan Chen, Di Li, Qing Huang,* and Chunhai Fan*

Laboratory of Physical Biology, Shanghai Institute of Applied Physics, Chinese Academy of Sciences, Shanghai 201800, China [†]These authors contributed equally to this work.

Nucleic acids are versatile materials for the “bottom-up” construction of exquisite nanostructures with high controllability and precision.^{1–3} Since the pioneering work of Seeman in the 1980s, there have been great advances in the area of DNA nanotechnology, in both directed assembly of highly complex nanostructures^{4–10} and promising applications of these nanostructures in molecular sensing,^{11–13} computation,^{14,15} and nanomachines.^{16–20} An elegant example is the cage-like DNA tetrahedral nanostructure originally developed by Turberfield and co-workers.^{21,22} Previous studies have proven that this three-dimensional nanostructure has excellent mechanical rigidity and structural stability. More significantly, this tetrahedral nanostructure can be rapidly and reliably assembled with four designed DNA oligonucleotides and easily functionalized with different chemical moieties and biomolecules. By exploiting these interesting properties, we previously devised a DNA tetrahedron-based platform for high-sensitivity *in vitro* sensing of a range of biomolecules.^{23,24} Very recently, Walsh *et al.* demonstrated that DNA tetrahedron can readily enter mammalian cell even in the absence of transfection reagents and remains substantially intact within the cytoplasm.²⁵ In this work, we aim to develop a functional DNA tetrahedron, that is, cell-permeable and highly immunostimulatory DNA nanostructures bearing unmethylated cytosine-phosphate-guanine (CpG) motifs.

Functional nucleic acids are single-stranded DNA or RNA sequences with unconventional ligand binding (e.g., aptamers^{26–28}),

ABSTRACT Designed oligonucleotides can self-assemble into DNA nanostructures with well-defined structures and uniform sizes, which provide unprecedented opportunities for biosensing, molecular imaging, and drug delivery. In this work, we have developed functional, multivalent DNA nanostructures by appending unmethylated CpG motifs to three-dimensional DNA tetrahedra. These small-sized functional nanostructures are compact, mechanically stable, and noncytotoxic. We have demonstrated that DNA nanostructures are resistant to nuclease degradation and remain substantially intact in fetal bovine serum and in cells for at least several hours. Significantly, these functional nanostructures can noninvasively and efficiently enter macrophage-like RAW264.7 cells without the aid of transfection agents. After they are taken up by cells, CpG motifs are recognized by the Toll-like receptor 9 (TLR9) that activates downstream pathways to induce immunostimulatory effects, producing high-level secretion of various pro-inflammatory cytokines including tumor necrosis factor (TNF)- α , interleukin (IL)-6, and IL-12. We also show that multivalent CpG motifs greatly enhance the immunostimulatory effect of the nanostructures. Given the high efficacy of these functional nanostructures and their noncytotoxic nature, we expect that DNA nanostructures will become a promising tool for targeted drug delivery.

KEYWORDS: DNA nanotechnology · tetrahedral · transfection · immunostimulation · nanomedicine

catalytic (e.g., DNAzymes^{29,30}), or physiological (e.g., CpG) properties. CpG oligodeoxynucleotides (ODNs) are a type of therapeutic nucleic acids with strong immunostimulatory activities.³¹ They are commonly present in natural viral and bacterial DNA, which are responsible for host immune responses to invading pathogens.^{32,33} Interestingly, synthetic CpG ODNs can bind to endosomal Toll-like receptor 9 (TLR9) and induce its conformational changes.³⁴ This recognition process allosterically activates TLR9, triggering a signaling cascade that leads to the remarkable immunostimulatory properties of CpG ODNs. Because of this, CpG ODNs have been actively explored in both basic research and clinical trials as a type of potent

* Address correspondence to
huangqing@sinap.ac.cn,
fchh@sinap.ac.cn.

Received for review July 21, 2011
and accepted October 11, 2011.

Published online October 11, 2011
10.1021/nn202774x

© 2011 American Chemical Society

and safe vaccine adjuvant for immunotherapy of infectious diseases and cancer.³⁵ Typical approaches to increase the efficacy of CpG ODNs include chemical modification of ODNs for resistance of enzymatic degradation^{36,37} and complexation of ODNs with cationic polymers or lipids for efficient cellular uptake,^{38–40} which nevertheless raise potential safety concerns.^{41,42} In a different approach, CpG-containing Y-shaped⁴³ or dendrimer-like DNA⁴⁴ and DNA hydrogels⁴⁵ have been designed to improve the activity without sacrificing biocompatibility. Given that DNA nanostructures are well-defined, structurally rigid, and inherently insensitive to nuclease degradation,^{46,47} we append CpG motifs to different vertices of DNA tetrahedron, evaluate the efficiency of cellular uptake and stability of these multivalently functionalized DNA nanostructures, and explore their immunoregulatory effects (Figure 1).

RESULTS AND DISCUSSION

The core DNA tetrahedral nanostructure can be readily assembled with four designed 55-mer strands (A–D, Table S1 in Supporting Information) with a simple annealing process.^{22,23} We prepare the CpG-bearing DNA tetrahedral nanostructure by using the sequences shown in Table S1, that is, the assembly sequence extended with the CpG sequence and a 7-mer oligothymine spacer. Nanostructures with different valence numbers of CpG were assembled with

the same protocol (Figures S1 and S2 in Supporting Information), which are named tetra-CpG(I), tetra-CpG(II), tetra-CpG(III), and tetra-CpG(IV). An analysis by gel electrophoresis exhibited one prominent band for each nanostructure (Figure S2b), and their mobility apparently decreased along with the valence number, suggesting that these functional nanostructures have been successfully constructed. Characterization of nanocages with melting curve analysis (Figure S3), fluorescence resonance energy transfer (FRET, Figure S4), and atomic force microscopy (AFM, Figure S5) showed a high degree of consistency between tetrahedron and tetra-CpGs, indicating that appending CpG motifs to tetrahedrons did not hinder the formation of their three-dimensional configuration. Also of note, due to the geometric simplicity of DNA tetrahedron, each nanostructure has only one single three-dimensional configuration without any isomers.

In order to study the cellular uptake ability of these nanostructures, we incubated macrophage-like RAW264.7 cells with 100 nM of DNA tetrahedral structures, containing one TAMRA-labeled strand A (see Table S1). We observed intense TAMRA fluorescence in cells with confocal fluorescence microscopy. These nanostructures were predominantly localized in the cytoplasm, as confirmed by costaining with Hoechst, a nuclei-specific dye (Figure 2). In contrast, control studies with 100 nM of TAMRA-labeled single-stranded (ss-) DNA (strand A) showed minimal fluorescence (Figure 2), suggesting that the presence of tetrahedral nanostructure is crucial for efficient intracellular delivery. Besides, the nonuniform distribution of dye-labeled DNA in cells indicated that these DNA structures were aggregated or segregated within certain organelles (e.g., lysosomes) in cells.²⁵ More details about their routes of entry will be investigated in our future studies.

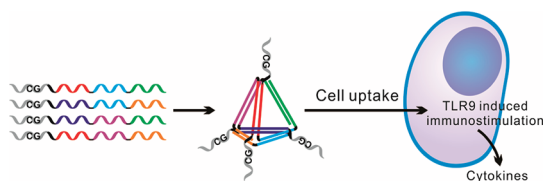


Figure 1. Schematic showing of the assembly of CpG-bearing DNA tetrahedron and its immunostimulatory effect.

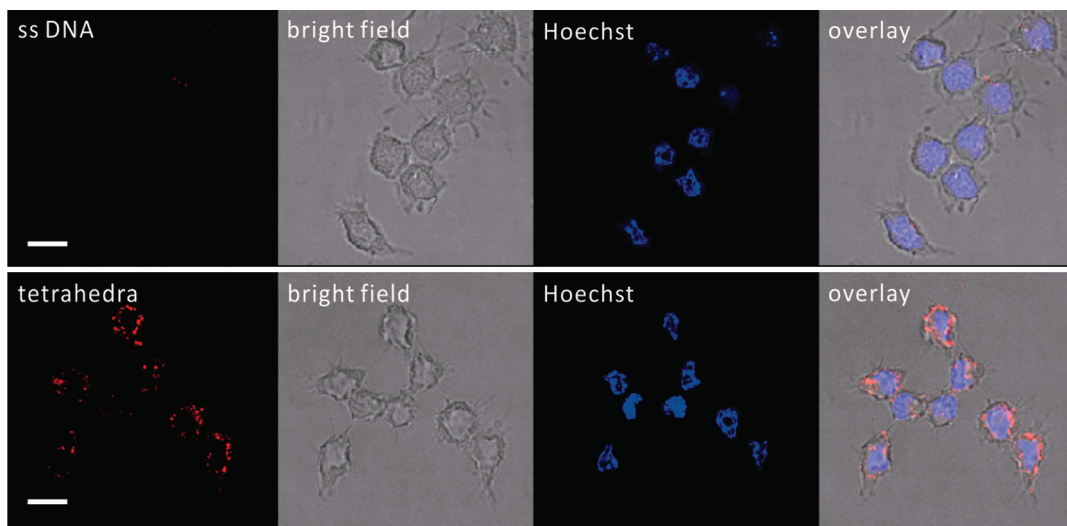


Figure 2. Confocal microscopic pictures for intracellular localization of TAMRA-labeled ssDNA (strand A) and DNA tetrahedra free of CpGs. Scale bars: 10 μ m.

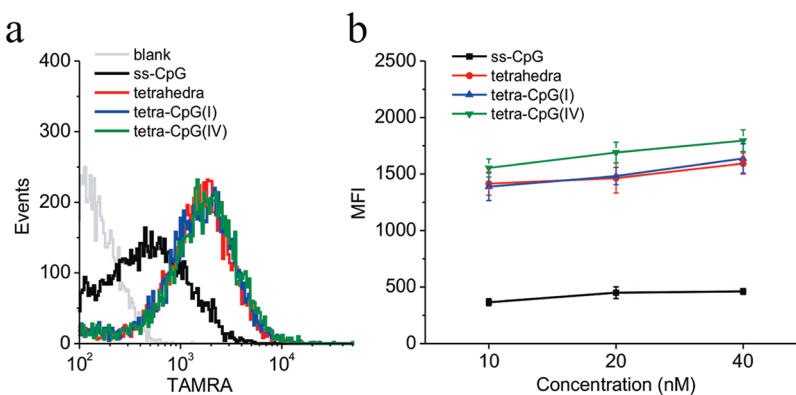


Figure 3. Flow cytometry analysis of cellular uptake. Cells were incubated with TAMRA-labeled ss-CpG ODN, CpG-free tetrahedron, tetra-CpG(I), and tetra-CpG(IV) for 2 h at 37 °C. (a) Overlaid histogram of cells treated with different DNA structures carrying 40 nM TAMRA-labeled DNA; (b) mean fluorescence intensity (MFI) plotted versus the concentration of labeled DNA, with the background MFI of blank cells subtracted. Error bars represent standard deviation (SD) of at least three independent measurements.

Flow cytometry analysis provides a quantitative approach for the evaluation of the cellular uptake efficiency. We employed ssDNA (strand A), CpG-free tetrahedron, and two CpG-bearing nanostructures, tetra-CpG(I) and tetra-CpG(IV), each labeled with TAMRA at the end of strand A, for incubation with RAW264.7 cells. As shown in Figure 3, the mean fluorescent intensity (MFI) for cells treated with all tetrahedral nanostructures was significantly higher than that of ssDNA, indicating the high cellular uptake efficiency of tetrahedral nanostructures. All three nanostructures showed similar efficiency, suggesting that the presence of CpG motifs and the variation of the valence number have little influence on the efficiency of cellular uptake.

DNA tetrahedral nanostructures have proven to be stable against nuclelease degradation in biological media. We incubated either DNA tetrahedron or partially complementary DNA duplexes (strand A + B) of the same concentration (500 nM) with 50% non-inactivated fetal bovine serum (FBS). Gel electrophoresis showed that the band for the nanostructure remained almost unchanged with 4 h incubation, reflecting the presence of intact tetrahedral nanostructure in FBS (Figure 4). Extended incubation led to smearing bands, suggesting partial degradation of the nanostructure. However, we note that the band for the nanostructure could still be observed with attenuated intensity even after 24 h incubation. In contrast, the DNA duplex was nearly completely degraded within only 2 h incubation, as expected for strong nuclease degradation in FBS. Moreover, colocalization studies with dual-labeled nanostructures (Cy3 and Cy5 labeled on different vertexes) showed that the two fluorescent colors were present nearly in the same place even after 8 h, which further confirms that DNA nanostructures are stable within cells (Figure 5). In addition, tetrahedrons labeled with FITC (fluorescein isothiocyanate) and TAMRA (tetramethylrhodamine) as a FRET pair on the same

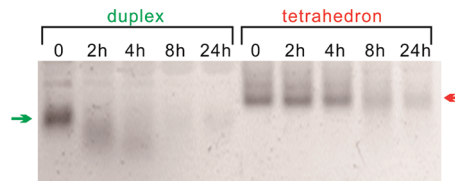


Figure 4. Electrophoretic analysis of the stability of DNA tetrahedral nanostructure. Partially complementary DNA duplex (strand A + B) and DNA tetrahedron were incubated in 50% non-heat-inactivated fetal bovine serum (FBS) at 37 °C for 2–24 h and then analyzed with gel electrophoresis.

vertex but different strands were also observed intracellularly after a 4 h incubation (Figure S6). An *in situ* wavelength scan of fluorescence emission showed an obvious sensitization of TAMRA (as an acceptor) caused by FRET, indicating that this pair of fluorophors was still close to each other, which was also a proof of conformational stability of these nanocages.

The cytotoxicity of DNA nanostructures was evaluated with a standard colorimetric MTT (3-(4,5-dimethylthiazol-2-yl)-2,5-diphenyl tetrazolium bromide) assay that assesses the metabolic activity of cells. We found that the tetrahedron did not induce measurable loss in the viability of cells even at a concentration of 0.1 μM, and that CpG-functionalized nanostructures even slightly stimulated the growth of cells (Figure 6). The latter effect might be due to the immunostimulatory activity of CpG motifs.⁴⁸

CpG ODNs are well-known to be immunostimulatory agents. They are recognized by Toll-like receptor 9 (TLR9) that activates downstream pathways to induce immunostimulatory effects, secreting various pro-inflammatory cytokines including tumor necrosis factor (TNF)-α, interleukin (IL)-6, and IL-12. We then incubated a single-stranded CpG ODN (80 nM) and a series of nanostructures (20 nM) with RAW264.7 cells for 8 h and measured the release of cytokines by using ELISA assays (raw data are presented in Supporting Information, Figure S8–S10 and Table S2). The CpG-free tetrahedron

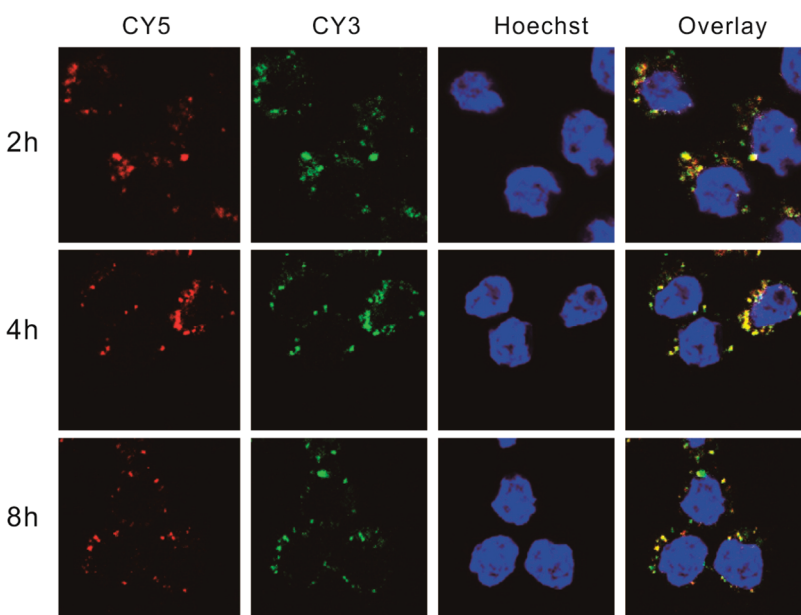


Figure 5. Colocalization studies of the stability of DNA tetrahedron with dual-labeled DNA tetrahedron.

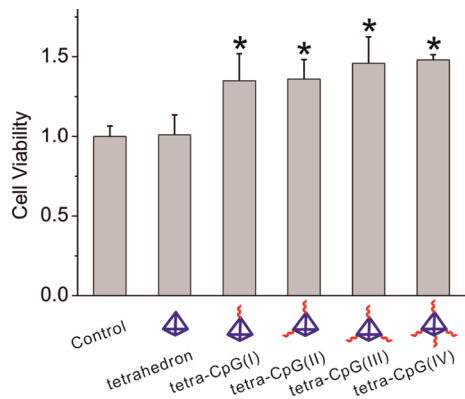


Figure 6. MTT assays of cell viability. DNA nanostructures of $0.1 \mu\text{M}$ were incubated with RAW264.7 cells for 24 h. Error bars represent standard deviation (SD) of at least three independent measurements. * $P < 0.05$ significantly different from the control.

had minimal stimulating activity for the production of TNF- α (Figure 7a). However, all CpG-modified nanostructures dramatically induced the production of TNF- α , excelling that of CpG ODN by 9–18 times. Even with the assistance of lipofectin, CpG ODN still had far less activity compared to CpG-bearing nanostructures. Similarly, the levels of other two cytokines, IL-6 (Figure 7b) and IL-12 (Figure 7c), were also greatly increased. This marked difference is primarily attributed to the greatly enhanced cellular uptake efficiency of nanostructures as compared to ssDNA. In addition, we found that the stimulating efficiency was increased when the valence number of CpG motifs was increased. It is worthwhile to point out that the presence of four CpG motifs is not the only reason for the highest stimulation effect observed for tetra-CpG(IV). When only 5 nM of tetra-CpG(IV) was employed (*i.e.*, with a molar concentration of a quarter

of tetra-CpG(I)s), it still stimulated 50% more TNF- α than tetra-CpG(I) (Figure S7). This suggests that tetra-CpG(IV) might possess higher affinity to TLR9 than tetra-CpG(I), possibly due to the presence of a collective effect of four CpG motifs.

ODNs have been actively exploited as promising therapeutic agents due to their high solubility, design flexibility, and good safety.^{35,45} However, naked ODNs are usually not efficiently cell-permeable in the absence of transfection agents (*e.g.*, lipofectin). Since tetrahedral nanostructures have small sizes ($\sim 6 \text{ nm}$) and compact structures, they have shown high cellular uptake efficiency.²⁵ Compared to other synthetic polymer agents (*e.g.*, cationic polymers)^{38,39,49} or inorganic nanoparticle carriers (*e.g.*, gold nanoparticles or carbon nanomaterials),^{50–55} these inherently nontoxic DNA nanostructures show comparatively excellent transfection abilities. The other important ability of DNA nanostructures is their resistance to nuclelease degradation, which effectively stabilizes CpG motifs in cells. More significantly, the presence of multivalent CpG motifs enhances the immunostimulatory activity. We find that tetra-CpG(IV) ($2 \mu\text{g}/\text{mL}$) induces the production of more than $100 \text{ pg}/\text{mL}$ IL-6, excelling that of dendrimer-like DNA structures (about $30 \text{ pg}/\text{mL}$) by more than 3-fold.⁴⁴ Therefore, DNA nanostructures have proven to be a promising carrier for intracellular delivery of CpG as well as other functional ODNs.

Besides cellular uptake efficiency and stability, several spatial factors might also contribute to the stimulatory activities of CpG-bearing nanostructures, which include the accessibility of CpGs' 5'-end,^{56,57} the self-stabilized secondary structure,^{58–60} and polyvalence of CpG motifs.^{44,60,61} The tetra-CpG(IV) satisfies many of these requirements and shows excellent

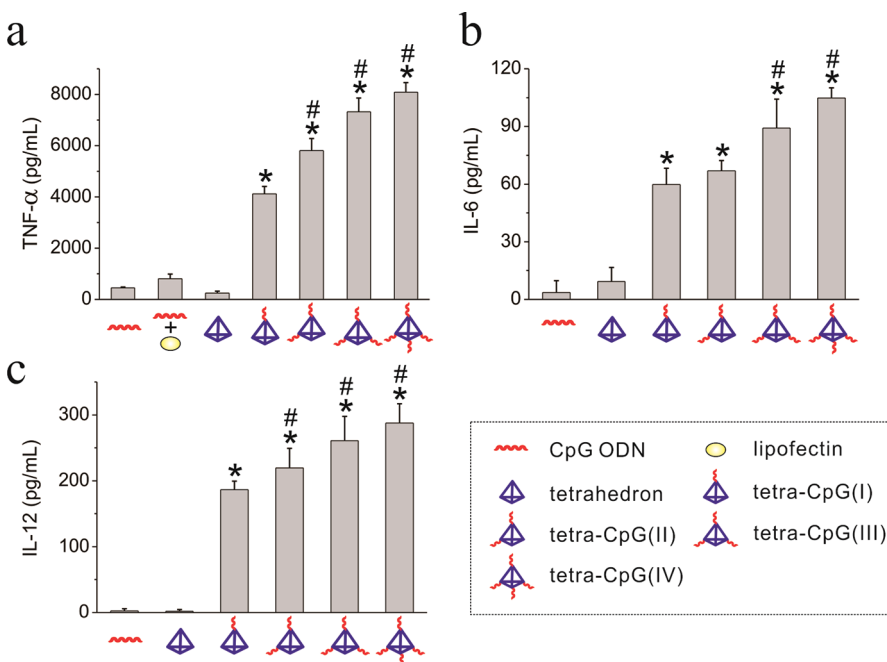


Figure 7. Cytokine release from RAW264.7 cells stimulated by DNA nanostructures. Comparison of (a) TNF- α , (b) IL-6, and (c) IL-12 release stimulated by CpG ODN (80 nM) and DNA nanostructures of 20 nM. Error bars represent standard deviation (SD) of at least three independent measurements. * $P < 0.001$ significantly different from CpG ODN and tetrahedron. # $P < 0.05$ significantly different from tetra-CpG(I).

immunostimulatory activity. Compared with previously reported Y-shaped or dendrimer-shaped DNA structures,⁴⁴ tetrahedral nanostructures not only are convenient to prepare with high yield but also provide a platform with small and compact structures that are easily cell-permeable.^{62–64} Moreover, since DNA nanostructures are of uniform sizes and precise structures, it is possible to accurately place CpG motifs to any specific positions of the tetrahedron with predefined numbers and sequence design. This precise tailorability is important for understanding the mechanism of the interactions between the nanostructures and TLR9, based on which one may further increase the efficacy of nanostructures. In addition, given that these cage-like nanostructures are hollow structures, it is possible to carry antitumor drugs such that the drugs and the

CpG motifs can synergistically inhibit the growth of tumors.

CONCLUSIONS

In this study, we have prepared functional DNA nanostructures by appending CpG motifs to DNA tetrahedra. We find that these nanostructures can be efficiently and noninvasively taken up by RAW264.7 cells. These nanostructures remain largely intact in cells for 8 h and dramatically induce the secretion of cytokines from these cells. We have also demonstrated that the multivalency of CpG is important for the immunostimulatory activity. Therefore, DNA tetrahedral nanostructures provide unprecedented opportunities to design uniform and safe drug delivery nanocarriers with precise structures, flexible tailorability, and high efficacy.

MATERIALS AND METHODS

Cell Cultures. RAW264.7 macrophage-like cells were grown in RPMI 1640 medium (Invitrogen) supplemented with 10% heat-inactivated FBS, 0.15% NaHCO₃, 100 units/mL penicillin, 100 mg/mL streptomycin, and 2 mM L-glutamine at 37 °C in humidified air containing 5% CO₂. Cells were then seeded on 24-well culture plates at a density of 5 × 10⁵ cells/mL and cultured for 24 h.

Preparation of Tetrahedral Nanostructures. DNA tetrahedral structures were prepared as reported previously.^{22,23} In brief, four designed strands (A–D) synthesized by TaKaRa Biotechnology (Dalian) Co., Ltd. were mixed in equimolar ratio in TM buffer (10 mM Tris-HCl, pH 8.0, 50 mM MgCl₂). The solution was heated to 95 °C for 5 min and then quickly cooled to 4 °C. Structures with various numbers of CpG side chains were

constructed by mixing different sets of strands as listed in Table S1 and Figure S1 in the Supporting Information.

Confocal Microscopic Imaging. Cell images were taken with a Leica confocal microscope setup. RAW264.7 cells were seeded on glass coverslips in 24-well culture plates at a density of 5 × 10⁵ cells/mL and incubated at 37 °C for 24 h. They were then washed twice with phosphate buffer (PBS) and incubated with fluorescently labeled DNA structures (for investigation of cellular uptake, TAMRA was labeled on strand A; for colocalization, Cy3 and Cy5 were separately labeled on strand A and B) in fresh RPMI 1640 medium for 2 h at 37 °C. Cells were then washed twice with PBS, fixed with 3% paraformaldehyde/sucrose, and the nuclei were stained using 3 µg/mL Hoechst 33258. The coverslips were mounted on a glass slide. All images were obtained using a laser confocal microscope (Leica TCS SP5).

Wavelength sets were 561 nm ex/570–600 nm for TAMRA, 561 nm ex/565–600 nm for Cy3, and 633 nm ex/650–690 nm for Cy5.

Uptake of DNA Nanostructures in RAW264.7 Cells. TAMRA-labeled A strand was used for the preparation of fluorescently labeled DNA nanostructures. RAW264.7 cells were seeded on 24-well culture plates at a density of 5×10^5 cells/mL and cultured for 24 h and then washed twice with PBS. They were incubated with fluorescently labeled DNA structures for 2 h at 37 °C, harvested, and washed three times with PBS. Then, the fluorescence intensity of the cells was determined by flow cytometry (FACSCarry; BD Biosciences, San Jose, CA, USA).

Cytokine Assays. RAW264.7 cells were washed twice with 0.5 mL of PBS before use. Then, DNA nanostructures of various concentrations were diluted with fresh medium and then added to cells. The cells were incubated at 37 °C for 8 h (for TNF- α analysis) or 24 h (for IL-6 and IL-12 analysis), and the supernatants were collected and stored at –80 °C until use. The levels of TNF- α , IL-6, and IL-12 in the supernatants were determined by enzyme-linked immunosorbent assay (ELISA) using antibody pairs specific to these cytokines (eBioscience, antimouse TNF- α pair, Cat. Nos. 14-7325 and 13-7326; antimouse IL-6 Pair, Cat. Nos. 14-7061 and 13-7062; antimouse IL-12 pair, Cat. Nos. 14-7125 and 13-7123), following protocols recommended by the manufacturer.

Statistical Analysis. Statistical differences of data were evaluated by one-way analysis of variance (ANOVA) followed by the Tukey's posthoc test for multiple comparisons. A *P* value of less than 0.05 was considered to be statistically significant.

Stability Analysis of DNA Nanostructures. Solutions of DNA nanostructures and single-strand DNA (unified to 67.7 μ g/mL) were separately mixed with non-heat-inactivated FBS of equal volume and incubated at 37 °C. After incubation of 0, 2, 4, 8, or 24 h, the mixtures were run on a 2% agarose gel and stained with ethidium bromide.

MTT Assays. Cytotoxicity was estimated using an MTT assay. Briefly, cells were seeded in 96-well plates and cultured overnight to reach ~80% confluence. Fresh media containing DNA nanostructures (100 nM) were incubated with cells for 24 h. Then, 20 μ L of 5 mg/mL thiazolyl blue tetrazolium bromide (MTT, Sigma-Aldrich, USA) solution was added to each well, followed by 4 h incubation at 37 °C. Next, cells were lysed with 10% acid SDS solution (pH 2–3). After centrifugation, the absorbance of supernatant was measured at 570 nm using a microplate reader (Bio-Rad 680, USA).

Acknowledgment. This work was supported by National Natural Science Foundation (20725516, 20873175, 90913014, and 21028005), Ministry of Science and Technology (2007CB936000), and Chinese Academy of Sciences.

Supporting Information Available: Oligonucleotide sequences used in this work, scheme for preparing DNA tetrahedron structures, AFM, melting curves, FRET studies, electrophoresis analysis of DNA structures, comparison of TNF- α releasing from RAW264.7 cells stimulated by tetra-CpG(I) and tetra-CpG(IV), raw data of ELISA detections of cytokines. This material is available free of charge via the Internet at <http://pubs.acs.org>.

REFERENCES AND NOTES

- Seeman, N. C. DNA in a Material World. *Nature* **2003**, *421*, 427–431.
- Rothenmund, P. W. K. Folding DNA To Create Nanoscale Shapes and Patterns. *Nature* **2006**, *440*, 297–302.
- Nangreave, J.; Han, D.; Liu, Y.; Yan, H. DNA Origami: A History and Current Perspective. *Curr. Opin. Chem. Biol.* **2010**, *14*, 608–615.
- Zhang, Y. W.; Seeman, N. C. Construction of a DNA-Truncated Octahedron. *J. Am. Chem. Soc.* **1994**, *116*, 1661–1669.
- Shih, W. M.; Dietz, H.; Douglas, S. M. Folding DNA into Twisted and Curved Nanoscale Shapes. *Science* **2009**, *325*, 725–730.
- Lin, C.; Liu, Y.; Yan, H. Designer DNA Nanoarchitectures. *Biochemistry* **2009**, *48*, 1663–1674.
- Shih, W. M.; Quispe, J. D.; Joyce, G. F. A 1.7-Kilobase Single-Stranded DNA That Folds into a Nanoscale Octahedron. *Nature* **2004**, *427*, 618–621.
- Han, D.; Pal, S.; Nangreave, J.; Deng, Z.; Liu, Y.; Yan, H. DNA Origami with Complex Curvatures in Three-Dimensional Space. *Science* **2011**, *332*, 342–346.
- Reif, J. H.; Majumder, U. M.; Rangnekar, A.; Gothelf, K. V.; Lassean, T. H. Design and Construction of Double-Decker Tile as a Route to Three-Dimensional Periodic Assembly of DNA. *J. Am. Chem. Soc.* **2011**, *133*, 3843–3845.
- Liedl, T.; Hogberg, B.; Tytell, J.; Ingber, D. E.; Shih, W. M. Self-Assembly of Three-Dimensional Prestressed Tensegrity Structures from DNA. *Nat. Nanotechnol.* **2010**, *5*, 520–524.
- Lin, C.; Katilius, E.; Liu, Y.; Zhang, J.; Yan, H. Self-Assembled Signaling Aptamer DNA Arrays for Protein Detection. *Angew. Chem., Int. Ed.* **2006**, *45*, 5296–5301.
- Zhang, Z.; Wang, Y.; Fan, C. H.; Li, C.; Li, Y.; Qian, L. L.; Fu, Y. M.; Shi, Y. H.; Hu, J.; He, L. Asymmetric DNA Origami for Spatially Addressable and Index-Free Solution-Phase DNA Chips. *Adv. Mater.* **2010**, *22*, 2672–2675.
- Zhang, Z.; Zeng, D. D.; Ma, H. W.; Feng, G. Y.; Hu, J.; He, L.; Li, C.; Fan, C. H. A DNA-Origami Chip Platform for Label-Free SNP Genotyping Using Toehold-Mediated Strand Displacement. *Small* **2010**, *6*, 1854–1858.
- Seeman, N. C. DNA Nanostructures for Mechanics and Computing: Nonlinear Thinking with Life's Central Molecule. In *NanoBiotechnology*; Wiley-VCH Verlag GmbH & Co. KGaA: Weinheim, Germany, 2005; pp 308–318.
- Winfree, E.; Qian, L. L. Scaling Up Digital Circuit Computation with DNA Strand Displacement Cascades. *Science* **2011**, *332*, 1196–1201.
- Gu, H. Z.; Chao, J.; Xiao, S. J.; Seeman, N. C. A Proximity-Based Programmable DNA Nanoscale Assembly Line. *Nature* **2010**, *465*, 202–U86.
- Lund, K.; Manzo, A. J.; Dabby, N.; Michelotti, N.; Johnson-Buck, A.; Nangreave, J.; Taylor, S.; Pei, R. J.; Stojanovic, M. N.; Walter, N. G.; et al. Molecular Robots Guided by Prescriptive Landscapes. *Nature* **2010**, *465*, 206–210.
- Omaghego, T.; Sha, R.; Seeman, N. C. A Bipedal DNA Brownian Motor with Coordinated Legs. *Science* **2009**, *324*, 67–71.
- Rotaru, A.; Gothelf, K. V. DNA Nanotechnology: Steps towards Automated Synthesis. *Nat. Nanotechnol.* **2010**, *5*, 760–761.
- Gothelf, K. V.; Zhang, Z.; Olsen, E. M.; Kryger, M.; Voigt, N. V.; Torring, T.; Gultekin, E.; Nielsen, M.; MohammadZadegan, R.; Andersen, E. S.; et al. A DNA Tile Actuator with Eleven Discrete States. *Angew. Chem., Int. Ed.* **2011**, *50*, 3983–3987.
- Goodman, R. P.; Schaap, I. A. T.; Tardin, C. F.; Erben, C. M.; Berry, R. M.; Schmidt, C. F.; Turberfield, A. J. Rapid Chiral Assembly of Rigid DNA Building Blocks for Molecular Nanofabrication. *Science* **2005**, *310*, 1661–1665.
- Goodman, R. P.; Berry, R. M.; Turberfield, A. J. The Single-Step Synthesis of a DNA Tetrahedron. *Chem. Commun.* **2004**, *1372*–1373.
- Pei, H.; Lu, N.; Wen, Y. L.; Song, S. P.; Liu, Y.; Yan, H.; Fan, C. H. A DNA Nanostructure-Based Biomolecular Probe Carrier Platform for Electrochemical Biosensing. *Adv. Mater.* **2010**, *22*, 4754–4758.
- Pei, H.; Wan, Y.; Li, J.; Hu, H. Y.; Su, Y.; Huang, Q.; Fan, C. H. Regenerable Electrochemical Immunological Sensing at DNA Nanostructure-Decorated Gold Surfaces. *Chem. Commun.* **2011**, *47*, 6254–6256.
- Walsh, A. S.; Yin, H.; Erben, C. M.; Wood, M. J. A.; Turberfield, A. J. DNA Cage Delivery to Mammalian Cells. *ACS Nano* **2011**, *5*, 5427–5432.
- Ellington, A. D.; Szostak, J. W. In Vitro Selection of RNA Molecules That Bind Specific Ligands. *Nature* **1990**, *346*, 818–822.
- Liu, X.; Yan, H.; Liu, Y.; Chang, Y. Targeted Cell–Cell Interactions by DNA Nanoscaffold-Templated Multivalent Bispecific Aptamers. *Small* **2011**, *7*, 1673–1682.
- Cao, Z.; Tong, R.; Mishra, A.; Xu, W.; Wong, G. C.; Cheng, J.; Lu, Y. Reversible Cell-Specific Drug Delivery with

- Aptamer-Functionalized Liposomes. *Angew. Chem., Int. Ed.* **2009**, *48*, 6494–6498.
29. Breaker, R. R. DNA Enzymes. *Nat. Biotechnol.* **1997**, *15*, 427–431.
30. Reif, J.; Sahu, S. Autonomous Programmable Nanorobotic Devices Using DNAzymes. In *DNA Computing*; Garzon, M.; Yan, H., Eds.; Springer: Berlin/Heidelberg; 2008; Vol. 4848, pp 66–78.
31. Vollmer, J.; Krieg, A. M. Immunotherapeutic Applications of CpG Oligodeoxynucleotide TLR9 Agonists. *Adv. Drug Delivery Rev.* **2009**, *61*, 195–204.
32. Hemmi, H.; Takeuchi, O.; Kawai, T.; Kaisho, T.; Sato, S.; Sanjo, H.; Matsumoto, M.; Hoshino, K.; Wagner, H.; Takeda, K.; et al. A Toll-like Receptor Recognizes Bacterial DNA. *Nature* **2000**, *408*, 740–745.
33. Krieg, A. M. CpG Motifs in Bacterial DNA and Their Immune Effects. *Annu. Rev. Immunol.* **2002**, *20*, 709–760.
34. Latz, E.; Verma, A.; Visintin, A.; Gong, M.; Sirois, C. M.; Klein, D. C.; Monks, B. G.; McKnight, C. J.; Lamphier, M. S.; Duprex, W. P.; et al. Ligand-Induced Conformational Changes Allosterically Activate Toll-like Receptor 9. *Nat. Immunol.* **2007**, *8*, 772–779.
35. Klinman, D. M. Immunotherapeutic Uses of CpG Oligodeoxynucleotides. *Nat. Rev. Immunol.* **2004**, *4*, 249–258.
36. Krieg, A. M.; Matson, S.; Fisher, E. Oligodeoxynucleotide Modifications Determine the Magnitude of B Cell Stimulation by CpG Motifs. *Antisense Nucleic Acid Drug Dev.* **1996**, *6*, 133–139.
37. Mutwiri, G. K.; Nichani, A. K.; Babiuk, S.; Babiuk, L. A. Strategies for Enhancing the Immunostimulatory Effects of CpG Oligodeoxynucleotides. *J. Controlled Release* **2004**, *97*, 1–17.
38. Morille, M.; Passirani, C.; Vonarbourg, A.; Clavreul, A.; Benoit, J. P. Progress in Developing Cationic Vectors for Non-viral Systemic Gene Therapy against Cancer. *Biomaterials* **2008**, *29*, 3477–3496.
39. Boussif, O.; Lezoualch, F.; Zanta, M. A.; Mergny, M. D.; Scherman, D.; Demeneix, B.; Behr, J. P. A Versatile Vector for Gene and Oligonucleotide Transfer into Cells in Culture and In-Vivo - Polyethylenimine. *Proc. Natl. Acad. Sci. U.S.A.* **1995**, *92*, 7297–7301.
40. Felgner, P. L.; Gadek, T. R.; Holm, M.; Roman, R.; Chan, H. W.; Wenz, M.; Northrop, J. P.; Ringold, G. M.; Danielsen, M. Lipofection: A Highly Efficient, Lipid-Mediated DNA-Transfection Procedure. *Proc. Natl. Acad. Sci. U.S.A.* **1987**, *84*, 7413–7417.
41. Lv, H. T.; Zhang, S. B.; Wang, B.; Cui, S. H.; Yan, J. Toxicity of Cationic Lipids and Cationic Polymers in Gene Delivery. *J. Controlled Release* **2006**, *114*, 100–109.
42. Nishikawa, M.; Rattanakiat, S.; Takakura, Y. DNA-Based Nano-Sized Systems for Pharmaceutical and Biomedical Applications. *Adv. Drug Delivery Rev.* **2010**, *62*, 626–632.
43. Nishikawa, M.; Matono, M.; Rattanakiat, S.; Matsuoka, N.; Takakura, Y. Enhanced Immunostimulatory Activity of Oligodeoxynucleotides by Y-Shape Formation. *Immunology* **2008**, *124*, 247–255.
44. Rattanakiat, S.; Nishikawa, M.; Funabashi, H.; Luo, D.; Takakura, Y. The Assembly of a Short Linear Natural Cytosine-Phosphate-Guanine DNA into Dendritic Structures and Its Effect on Immunostimulatory Activity. *Biomaterials* **2009**, *30*, 5701–5706.
45. Nishikawa, M.; Mizuno, Y.; Mohri, K.; Matsuoka, N.; Rattanakiat, S.; Takahashi, Y.; Funabashi, H.; Luo, D.; Takakura, Y. Biodegradable CpG DNA Hydrogels for Sustained Delivery of Doxorubicin and Immunostimulatory Signals in Tumor-Bearing Mice. *Biomaterials* **2011**, *32*, 488–494.
46. Mei, Q. A.; Wei, X. X.; Su, F. Y.; Liu, Y.; Youngbull, C.; Johnson, R.; Lindsay, S.; Yan, H.; Meldrum, D. Stability of DNA Origami Nanoarrays in Cell Lysate. *Nano Lett.* **2011**, *11*, 1477–1482.
47. Keum, J. W.; Bermudez, H. Enhanced Resistance of DNA Nanostructures to Enzymatic Digestion. *Chem. Commun.* **2009**, *7036*–7038.
48. Hartmann, G.; Weiner, G. J.; Krieg, A. M. CpG DNA: A Potent Signal for Growth, Activation, and Maturation of Human Dendritic Cells. *Proc. Natl. Acad. Sci. U.S.A.* **1999**, *96*, 9305–9310.
49. Pack, D. W.; Hoffman, A. S.; Pun, S.; Stayton, P. S. Design and Development of Polymers for Gene Delivery. *Nat. Rev. Drug Discovery* **2005**, *4*, 581–593.
50. Rosi, N. L.; Giljohann, D. A.; Thaxton, C. S.; Lytton-Jean, A. K.; Han, M. S.; Mirkin, C. A. Oligonucleotide-Modified Gold Nanoparticles for Intracellular Gene Regulation. *Science* **2006**, *312*, 1027–1030.
51. Kam, N. W.; Liu, Z.; Dai, H. Functionalization of Carbon Nanotubes via Cleavable Disulfide Bonds for Efficient Intracellular Delivery of siRNA and Potent Gene Silencing. *J. Am. Chem. Soc.* **2005**, *127*, 12492–12493.
52. Seferos, D. S.; Giljohann, D. A.; Hill, H. D.; Prigodich, A. E.; Mirkin, C. A. Nano-Flares: Probes for Transfection and mRNA Detection in Living Cells. *J. Am. Chem. Soc.* **2007**, *129*, 15477–15479.
53. Kam, N. W. S.; Liu, Z. A.; Dai, H. J. Carbon Nanotubes as Intracellular Transporters for Proteins and DNA: An Investigation of the Uptake Mechanism and Pathway. *Angew. Chem., Int. Ed.* **2006**, *45*, 577–581.
54. Lin, C. A.; Yang, T. Y.; Lee, C. H.; Huang, S. H.; Sperling, R. A.; Zanella, M.; Li, J. K.; Shen, J. L.; Wang, H. H.; Yeh, H. I.; et al. Synthesis, Characterization, and Bioconjugation of Fluorescent Gold Nanoclusters toward Biological Labeling Applications. *ACS Nano* **2009**, *3*, 395–401.
55. Wang, Z.; Zhang, J.; Ekman, J. M.; Kenis, P. J.; Lu, Y. DNA-Mediated Control of Metal Nanoparticle Shape: One-Pot Synthesis and Cellular Uptake of Highly Stable and Functional Gold Nanoflowers. *Nano Lett.* **2010**, *10*, 1886–1891.
56. Kandimalla, E. R.; Bhagat, L.; Yu, D.; Cong, Y. P.; Tang, J.; Agrawal, S. Conjugation of Ligands at the 5'-End of CpG DNA Affects Immunostimulatory Activity. *Bioconjugate Chem.* **2002**, *13*, 966–974.
57. Yu, D.; Zhao, Q.; Kandimalla, E. R.; Agrawal, S. Accessible 5'-End of CpG-Containing Phosphorothioate Oligodeoxynucleotides Is Essential for Immunostimulatory Activity. *Bioorg. Med. Chem. Lett.* **2000**, *10*, 2585–2588.
58. Cong, Y. P.; Song, S. S.; Bhagat, L.; Pandey, R. K.; Yu, D.; Kandimalla, E. R.; Agrawal, S. Self-Stabilized CpG DNAs Optimally Activate Human B Cells and Plasmacytoid Dendritic Cells. *Biochem. Biophys. Res. Commun.* **2003**, *310*, 1133–1139.
59. Kandimalla, E. R.; Bhagat, L.; Cong, Y. P.; Pandey, R. K.; Yu, D.; Zhao, Q. Y.; Agrawal, S. Secondary Structures in CpG Oligonucleotides Affect Immunostimulatory Activity. *Biochem. Biophys. Res. Commun.* **2003**, *306*, 948–953.
60. Wu, C. C.; Lee, J.; Raz, E.; Corr, M.; Carson, D. A. Necessity of Oligonucleotide Aggregation for Toll-like Receptor 9 Activation. *J. Biol. Chem.* **2004**, *279*, 33071–33078.
61. Minari, J.; Shimada, N.; Sakurai, K. Clustered CpG Sequences To Enhance Cytokine Secretion from Macrophages. *Chem. Lett.* **2008**, *37*, 92–93.
62. Aoyama, Y.; Kanamori, T.; Nakai, T.; Sasaki, T.; Horiuchi, S.; Sando, S.; Niidome, T. Artificial Viruses and Their Application to Gene Delivery. Size-Controlled Gene Coating with Glycocluster Nanoparticles. *J. Am. Chem. Soc.* **2003**, *125*, 3455–3457.
63. Osaki, F.; Kanamori, T.; Sando, S.; Sera, T.; Aoyama, Y. A Quantum Dot Conjugated Sugar Ball and Its Cellular Uptake. On the Size Effects of Endocytosis in the Subviral Region. *J. Am. Chem. Soc.* **2004**, *126*, 6520–6521.
64. Gao, H. J.; Shi, W. D.; Freund, L. B. Mechanics of Receptor-Mediated Endocytosis. *Proc. Natl. Acad. Sci. U.S.A.* **2005**, *102*, 9469–9474.